Pseudohalide Ions as Ligands to Tune Architecture and Luminescence of Polymetallic CU(I) Assemblies

Constance Lecourt, Sayed Muktar Hossain, Chendong Xu, Ali Mustafa Khalil, Guillaume Calvez, Smail Triki, Christophe Lescop

PSEUDOHALIDE IONS AS LIGANDS TO TUNE ARCHITECTURE AND LUMINESCENCE OF POLYMETALLIC CU(I) ASSEMBLIES

Constance Lecourt,[1] Sayed Muktar Hossain,[2] Chendong Xu,[1] Ali Mustafa Khalil,[1] Guillaume Calvez,[1] Smail Triki,[2]* Christophe Lescop[1]*

1 :Univ Rennes, INSA Rennes, CNRS, ISCR (Institut des Sciences Chimiques de Rennes) – UMR 6226, F-35000 Rennes, France. E-mail: christophe.lescop@insa-rennes.fr

2 :Univ Brest, CNRS, CEMCA, 6 Avenue Victor Le Gorgeu, C.S. 93837, 29238 Brest Cedex 3, France. E-mail: smail.triki@univ-brest.fr

ABSTRACT

The reaction of pre-assembled Cu(I) bimetallic units $\{Cu_2(dppm)_2\}$ and $\{Cu_2(dppa)_2\}$ (dppm: bis(diphenylphosphino)methane and dppa: bis(diphenylphosphino)amine) with pseudohalide linkers (azido, dicyanamide and tricyanomethanide) allows the quantitative and selective preparation of three discrete tetrametallic metallacycles of formula $[Cu_4(\mu_2\text{-}dppm)_4(N_3)_2](PF_6)_2$, $[Cu_4(\mu_2\text{-}dppm)_4(N(CN)_2)_2](PF_6)_2$ and $[Cu_4(\mu_2\text{-}dppm)_4((C(CN)_3)_4]$. To explore further the impact of the linker on the architecture and dimensionality of the molecular edifice, the study was extended to more sophisticated tetradentate cyanocarbanion ligands (tcnsMe$^-$: 2-(methylthio)-1,1,3,3-propanetetracarbonitrile and tcnsEt$^-$: 2-(ethylthio)-1,1,3,3-propanetetracarbonitrile). Three ladder-like one-dimensional coordination polymers and an octametallic metallacycle have been obtained. The careful comparison of the metric and geometrical intramolecular and intermolecular parameters observed in this series of seven derivatives allows to rationalize their molecular architectures. The subtle balance between the length and steric hindrance of the ligand and the formation of non-covalent interaction networks greatly influences the topology and dimensionality of the resulting assemblies and will be

discussed hereafter. The photophysical properties of these seven polymetallic Cu(I) compounds have been also studied.

INTRODUCTION

A fruitful synthetic approach for constructing complex molecular assemblies consists in the spontaneous association of rationally designed individual building blocks into well-defined supramolecular architectures. Considering more particularly the use of the metal-ligand coordination interaction to connect the building blocks, the coordination driven supramolecular (CDS) chemistry approach has been conceptualized,[1–4] consisting in the use of pre-organized coordination complexes having predefined geometries (being in most cases not accessible from single metal center coordination sphere) and vacant coordination positions. It has allowed the challenging preparation of a plethora of polymetallic advanced supramolecular architectures bearing increased structural complexity and new functionalities. In this powerful bottom-up approach, the desired sizes and geometries of the scaffolds obtained are defined and controlled by the symmetry of the linking sites of the individual building blocks. Therefore, in complement of the selection of the polytopic rigid connecting ligands, this approach presents a preference for Pd(II) and Pt(II) metal centers that combine rigid square planar coordination sphere and highly directional metal-ligand interactions with a large range of ligating coordination groups.[3,5–7]

However, after pioneering works, alternatives have highlighted the use of a larger variety of metal centers and connecting ligands' scaffolds[8–10] allowing significant degrees of conformational flexibility, and questioning somehow the initial 'rigidity' paradigms. This revealed the importance of secondary non-convalent interactions (such as metallophilic, π-π or π-CH interactions) in the selection of thermodynamic stable products that are prepared. In this

context, we have used pre-assembled Cu(I) precursors such as the {$Cu_2(\mu_2$-dppm$)_2$} bimetallic fragment **A** (Scheme 1, dppm = bis(diphenylphosphino)methane) in self-assembly procedures adapted from the CDS syntheses' principles.[11–15] We observed that the typical labile, flexible and low-directional coordination sphere of the Cu(I) ion, initially regarded *a priori* as strongly restrictive in conventional CDS chemistry, turned out to be very effective to conduct the selective preparation of polymetallic assemblies based on this ion. Thus, we described the selective preparation of the sterically constrained and highly emissive tetrametallic Cu(I) metallacycle **B** bearing cuprophilic interactions (Scheme 1; it is generally admitted that such interactions are characterized by intermetallic Cu(I)-Cu(I) distance below 2.8 Å[16]) from the self-assembly reaction of the precursor **A** with cyanide connecting ligands.[12] This thermodynamically stable tetrametallic assembly presents multiple chelates and metallacycle subunits embedding Cu(I) ions whose flexible coordination sphere geometry can be advantageously adapted to the topology constraints induced in such scaffolds. Importantly, coordinatively unsaturated distorted trigonal planar Cu(I) ions are present within the {$Cu_2(\mu_2$-dppm$)_2$} subunits **A**. In this scaffold, the metal ions keep a significant degree of flexibility allowing the metal centers to evolve to tetrahedral metal centers upon coordination of additional donor ligand, making of compound **B** an appealing precursor that allowed for selective preparation of a large variety of polymetallic Cu(I) assemblies. (Scheme 2).[12,13,17]

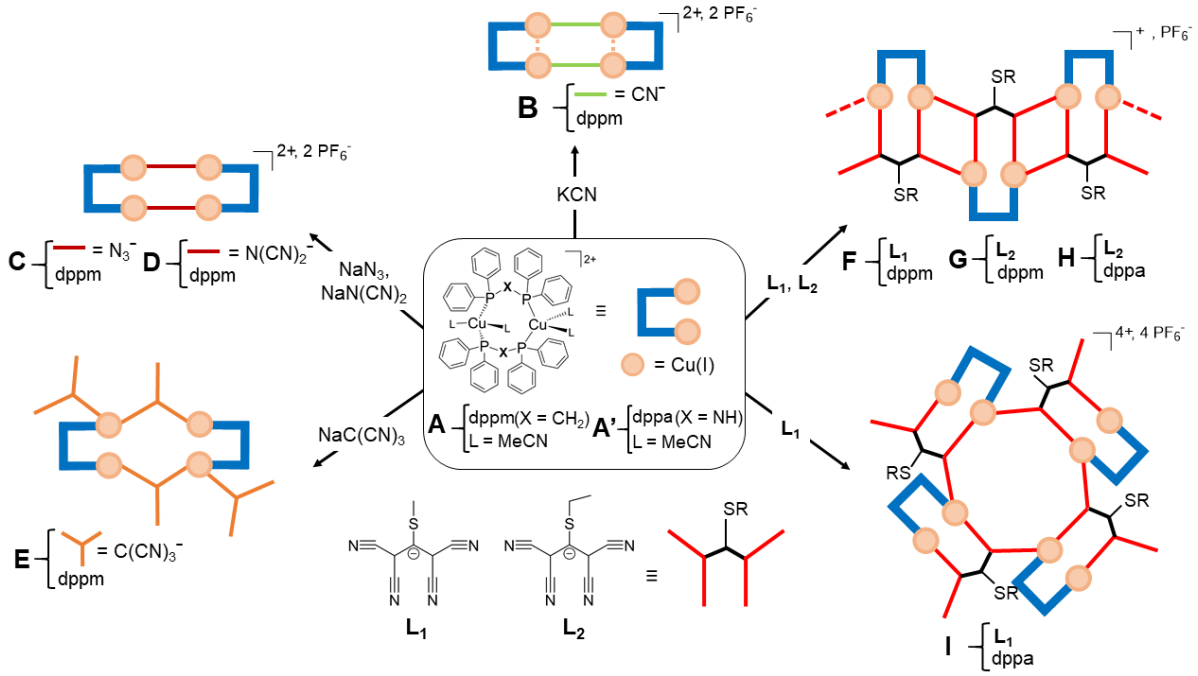

Scheme 1: Syntheses and schematic representation of derivatives **A-I** and ligands **L_1-L_2**

A very attractive facet of coordination compounds based on the Cu(I) ion concerns luminescence behaviors. Their emission properties cover the full visible light spectrum, combined with a large diversity of the radiative relaxation pathways including, but not only, very efficient Thermally Activated Delayed Fluorescence (TADF) processes.[18–24] In such complexes, spatially well separated HOMO and LUMO orbitals induce small lowest energy singlet-triplet energy gap allowing, *via* a reverse intersystem crossing (RISC), thermal population of the lowest energy excited singlet state (S_1) from the lowest energy triplet excited state (T_1). This induces efficient radiative relaxation to the ground state and exalted solid-state luminescence properties at temperatures close to room temperature (RT). It was initially considered that the high flexibility of the coordination sphere of the Cu(I) ion could be highly detrimental for the observation of exalted luminescence properties since it would promote major structural reorganizations in the excited states associated with detrimental efficient vibration modes, favoring the emergence of dominant non-radiative relaxation pathways. However, due to the use of specific bulky ligands, a great structural rigidity was imposed to highly sterically

encumbered Cu(I) metal centers, allowing observation of exalted luminescence properties in the resulting complexes. An alternative approach was introduced by Yam and Lescop with the adaptation of coordination-driven supra-molecular (CDS) synthetic principles to the use of the bimetallic Cu(I) flexible building-block **A** (Scheme 1).[12–14,25] It allowed the selective preparation of highly emissive TADF blue luminophore tetrametallic Cu(I) metallacycle **B** bearing cuprophilic interactions, a derivative that revealed also to be an appealing precursor toward preparation of original luminescent polymetallic assemblies. Importantly, in the tetrametallic Cu(I) metallacycle **B** and the related polymetallic assemblies (**1**-**6**) obtained from this precursor (Scheme 2),[12,13,17] the intrinsic significant scaffold rigidity imposed by the polycyclic CDS structures, promotes the occurrence of RT luminescence properties. For instance, the derivative **B** reveals to be an efficient TADF luminophore, emitting an eye-perceived blue light upon photoexcitation with a remarkable RT emission quantum yield of 72 %.

Aiming to explore further the relationship between the high conformational flexibility exhibited by Cu(I) CDS polymetallic assemblies and their luminescence properties, we herein extend our investigations by replacing the connecting cyanido ligands initially reacted with the {$Cu_2(\mu_2$-dppm$)_2$} subunit to obtain the metallacycle **B**. Therefore, we have reacted this {$Cu_2(\mu_2$-dppm$)_2$} bimetallic fragment with azido N_3^-, dicyanamide $N(CN)_2^-$ (dca^-), and tricyanomethanide $C(CN)_3^-$ (tcm^-) anions) (Scheme 1). In addition, these studies further stretched to the use of more sophisticated ($tcnsR^-$) cyanocarbanions which are able to act as polybridging ligands, ranging from μ_1 to μ_4 coordination modes (**L1** ($tcnsMe^-$) = 2-(methylthio)-1,1,3,3-propanetetracarbonitrile); **L2** ($tcnsEt^-$) = 2-(ethylthio)-1,1,3,3-propanetetracarbonitrile). **L1** and **L2** ligands were reacted with the precursor **A** and later with the {$Cu_2(\mu_2$-dppa$)_2$} bimetallic fragment **A'** (dppa = bis(diphenylphosphino)amine) (Scheme 1). As a result of these investigations, we report the syntheses, characterizations, X-ray single crystal molecular

structures and solid-state luminescence properties of seven new Cu(I) polymetallic assemblies **C-I**.

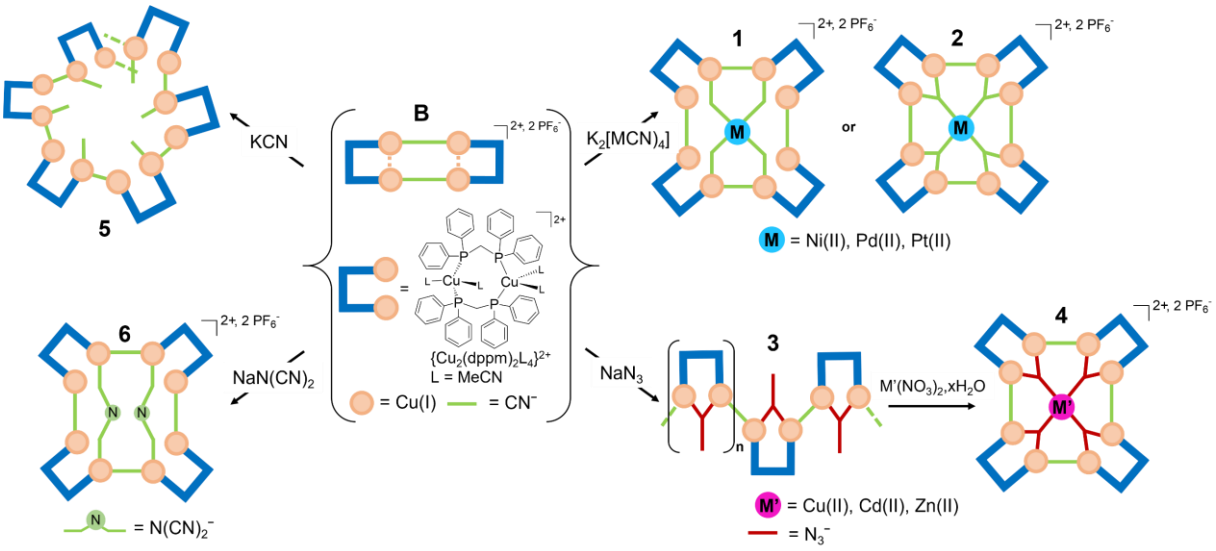

Scheme 2: Preparation and schematic representation of the derivative **B**[12] and the polymetallic assemblies **1-6** obtained from this pre-assembled precursor.

RESULTS AND DISCUSSION

Synthesis and crystal structure:

The reaction of two equivalents of diphosphine ligands (dppm and dppa) with two equivalents of $[Cu(CH_3CN)_4]PF_6$ in CH_2Cl_2 or THF at RT afforded *in situ* the bimetallic complexes **A** and **A'** respectively (Scheme 1). The molecular-clip precursor **A** was subsequently treated with one equivalent of pseudohalide linkers (N_3^-, dca^- or tcm^-) dissolved in MeOH (Scheme 1) (So far, reacting these linkers with **A'** did not allow selective preparation of identified new species). The resulting homogeneous clear colorless mixtures were vigorously stirred for 2 hours at room temperature and then filtered. Homogeneous batches of single crystals were obtained at RT from slow pentane or diethyl ether vapor diffusion into the mother solutions affording ionic derivatives $[Cu_4(\mu_2\text{-dppm})_4(N_3)_2](PF_6)_2$ (**C**), $[Cu_4(\mu_2\text{-dppm})_4(N(CN)_2](PF_6)_2$ (**D**) and the neutral assembly $[Cu_4(\mu_2\text{-dppm})_4((C(CN)_3)_4]$ (**E**). The $^{31}P\{^1H\}$ NMR spectra of the derivatives **C** and

D in CD_2Cl_2 display broad singlet at - 9.51 ppm and - 10.6 ppm respectively due to diphosphine unit. Besides these resonances, a characteristic septet signal was observed due to the PF_6^- ion (δ = - 144.6 ppm, $J_{P,F}$ = 706 Hz) that reveals the cationic nature of the Cu(I)-based assemblies (**C** and **D**) obtained (Figures S10-S12). Conversely, the $^{31}P\{^1H\}$ NMR spectrum of the derivative **E** in CD_2Cl_2 only displays a broad singlet at - 14.3 ppm, without any signal typical of the PF_6^- ion, suggesting a neutral Cu(I)-based derivative (Figure S14).

Table 1. Crystallographic data of derivatives **C**–**E**

	C	**D**	**E**
Empirical formula	$C_{54}H_{52}Cu_2F_6N_3OP_5$	$C_{104}H_{88}ClCu_4F_{12}N_6P_{10}$	$C_{58}H_{44}ClCu_2N_6P_4$
Formula weight ($g.mol^{-1}$)	1154.92	2213.66	1075.95
Temperature (K)	150(2)	150(2)	150(2)
Crystal system	Monoclinic	Monoclinic	Monoclinic
Space group	$P2_1/n$	$P2_1/n$	$P2_1/n$
a (Å)	14.690(1)	16.281(3)	17.515(1)
b (Å)	27.075(2)	20.440(3)	18.759(2)
*c (*Å)	15.048(2)	17.679(3)	17.642(1)
α (°)	90	90	90
β (°)	95.325(3)	108.198(5)	92.475(2)
γ (°)	90	90	90
V ($Å^3$)	5959.2(10)	5589.1(3)	5791.1(8)
Z	4	2	4
ρ_{calc} (g/cm^3)	1.287	1.315	1.234
μ (mm^{-1})	0.904	0.959	0.885
F(000)	2368.0	2256.0	2208.0
Crystal size (mm^3)	0.19 × 0.11 × 0.07	0.17 × 0.1 × 0.08	0.18 × 0.15 × 0.10
Radiation	MoKα (λ = 0.71069)	MoKα (λ = 0.71069)	MoKα (λ = 0.71069)
2Θ range for data collection/°	3.00 to 55.08	2.98 to 55.02	3.18 to 52.88
Index ranges	-19 ≤ h ≤ 19 -34 ≤ k ≤ 35 -16 ≤ l ≤ 19	-21 ≤ h ≤ 18 -26 ≤ k ≤ 26 -22 ≤ l ≤ 22	-21 ≤ h ≤ 21 -14 ≤ k ≤ 23 -19 ≤ l ≤ 22
Reflections collected	39839	45424	47968
Independent reflections	13639	12703	11841
Data/restraints/ parameters	13639/0/641	12703/0/643	11841/0/632
Goof on F^2	0.929	0.966	0.944

Final R[(a)] indexes [I≥2σ (I)] ωR[(b)] [I>2σ(I)]	R_1 = 0.0598 ωR_2 = 0.1525	R_1 = 0.0879 ωR_2 = 0.2278	R_1 = 0.0429 ωR_2 = 0.1162
Final R indexes (all data)	R_1 = 0.1018 ωR_2 = 0.1692	R_1 = 0.1566 ωR_2 = 0.2596	R_1 = 0.0636 ωR_2 = 0.1250
Largest diff. peak/hole (e.Å^{-3})	0.70/-0.62	1.73/-0.62	0.69/-0.33
CCDC number	2305990	2305989	2305991

[(a)] $R = \Sigma||Fo|-|Fc||/\Sigma|Fo|$, [(b)] $\omega R = [\Sigma(\omega(Fo^2-Fc^2)^2)/\Sigma(\omega(Fo^2)^2)]^{1/2}$ with $\omega = 1/[(\sigma^2Fo^2)+(aP)^2+bP]$ and $P = (max(Fo^2)+2Fc^2)/3$

Such chemical shifts range closely similar to the signal recorded for the derivative **B** (two broad singlets at - 8.5 and - 10.5 ppm) and suggest that the initial {$Cu_2(\mu_2$-dppm$)_2$} moieties are maintained in all compounds. In the room temperature ^{1}H NMR spectra, signals typical of the phenyl and the methylene protons of the dppm ligands (Figures S9-S11-S13) are observed. Worth to note, no signals due to coordinated CH_3CN ligands are present, and the infrared (IR) spectra of derivatives **C**, **D**, and **E** reveal the presence of pseudohalide linker groups ($\nu(N_3^-)$ = 2097 cm^{-1}; $\nu(N(CN)_2^-)$ = 2179 cm^{-1}; $\nu(C(CN)_3^-)$ = 2148-2187 cm^{-1}, Figures S25- - S27). Interestingly, in agreement with the NMR measurements, the PF_6^- anions were detected only in the solid-state IR spectra of the assemblies **C** and **D** ($\upsilon(PF_6^-)$ = 831 and 827 cm^{-1} respectively). Altogether, these spectroscopic data suggest that a substitution of the labile acetonitrile ligands of the Cu(I)-dimer **A** by azido linker (**C**) or by the 'C≡N' ligating moieties of the dca^- or tcm^- anions (**D** and **E**, respectively) occurs in these reactions affording cationic (**C** and **D**) and neutral (**E**) metallacycle assemblies. The molecular structures of compounds **C**, **D** and **E** were definitively established by single-crystal X-ray diffraction studies at 150 K (Table 1). Single crystals suitable for such analyses were obtained from pentane or diethyl ether vapor diffusions within THF solution for derivative **C** and within CH_2Cl_2 solutions for derivatives **D** and **E**. The colorless block crystals of derivatives **C**, **D** and **E** crystallize in the same $P2_1/n$ monoclinic space group. These species can be described as based on tetrametallic metallacycles of general formula **C**: [$Cu_4(\mu_2$-dppm$)_4(N_3)_2$]$(PF_6)_2$, **D**: [$Cu_4(\mu_2$-dppm$)_4(N(CN)_2$]$(PF_6)_2$ and **E**:

[$Cu_4(\mu_2$-dppm$)_4$((C(CN)$_3)_4$], resulting from the connection of two {$Cu_2(\mu_2$-dppm$)_2$} fragments by two pseudohalide ligands acting as ditopic linkers.

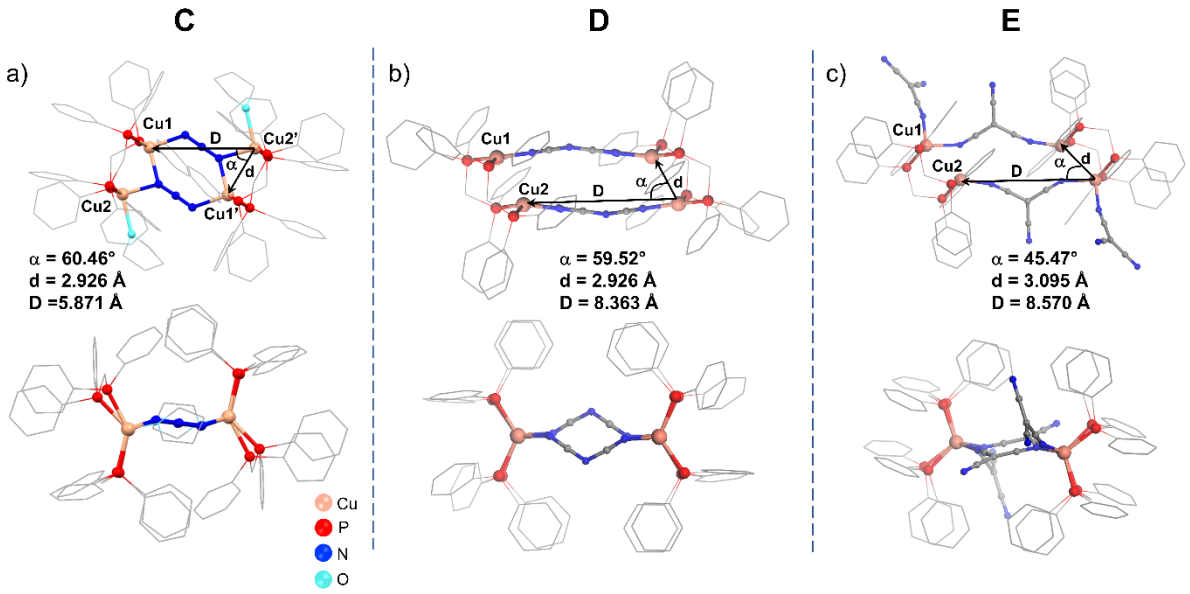

Figure 1. 'Top' and 'side' views of the molecular X-ray structures of the dicationic derivatives a) **C**, b) **D** and c) the neutral assembly **E**. H atoms, counter-anions and included solvent molecules have been omitted for clarity.

In these three derivatives, the four Cu(I) centers lie in the same plane defining centrosymmetric metallacycles. Regarding first the ionic assemblies **C** and **D**, for compound **C** the asymmetric unit contains one half of a metallacycle, one PF_6^- anion and one THF solvent molecule weakly coordinated to one copper center (d(Cu–O) = 2.302(3) Å), the entire supramolecular assemblies being generated *via* symmetry operation associated with the $P2_1/n$ space group. The asymmetric unit of compound **D** is mostly similar to the one in **C** but no coordinated solvent molecule is observed. Counter-ions are located outside the self-assembled structure and interact weakly with the phenyl groups of the dppm ligands. The Cu···Cu distances within the dicationic {$Cu_2(\mu_2$-dppm$)_2$} cores (3.0128(10) Å (**C**) and 2.9256(9) Å (**D**), Table 2) are longer than observed in the crystal structure of the analogous tetrametallic metallacycle **B** (2.8670(6) Å).[12] The intermetallic distance for the compound **D** is close to the upper limit of 2.8 Å generally considered for cuprophilic interactions.[16,26] In compound **C**, the azido linkers are adopting a $\mu_{1,1,3}$ coordination mode, with on one side a semi-bridging nitrogen atom (Table 2, d(Cu2-N) =

2.096(3) Å and d(Cu1-N) = 2.146(3) Å) that connects the two Cu1 and Cu2 centers of the {$Cu_2(\mu_2$-$dppm_2$)} core, and on the other side one nitrogen atom that is connected only to the Cu1' ion (d(Cu1-N) = 2.114(3) Å, **Figure 1**a). Therefore, the Cu1 metal centers present a distorted P_2N_2 tetrahedral coordination sphere while the Cu2 centers have a distorted $P_2N_1O_1$ tetrahedral coordination sphere (as a result of the weak coordination of a THF solvent molecule). The azido linkers in the metallacycle are parallel to each other and they are slightly deviated from the plane defined by the four metal centers, inducing a chair-like conformation to the central cyclic fragment (N1–Cu1–N3 = 94.10°, **Figure 1**a). In compound **D**, the dca^- anions are bridging the Cu1 and Cu2 centers of each fragment in end-on/end-on fashion with terminal coordinated atoms coordinated to a single metal center, similarly than in the compound **B** (Cu1 ions are located at the vertices of the acute angles and Cu2 ions are at the vertices of the obtuse angles of the tetrametallic metallacycle **D**, **Figure 1**b) with the central nitrogen atoms of these linkers being free from any coordination on a metal center.

Table 2. Selected bond lengths [Å] and angles [°] of the supramolecular assemblies **B–E**

	B[12]	**C**	**D**	**E**
Cu–P	2.243(1) 2.264(1) 2.259(1) 2.256(7)	2.2585(12) 2.2438(13) 2.2588(12) 2.2491(13)	2.2505(13) 2.2359(13) 2.2557(14) 2.2438(14)	2.2562(9) 2.2634(9) 2.2408(9) 2.2362(9)
Cu–N/C	1.92(2) 2.00(3)	2.114(3) 2.146(3) 2.096(3)	1.9190(6) 1.9457(6)	2.162(3) 2.012(2) 2.007(2)
Cu···Cu	2.867(1)	3.0128(10)	2.9256(9)	3.0948(5)
Cu–Cu–N/C	67.9(7) 130.0(9)	44.09(8) 138.2(1)	66.29 126.41	47.65(7) 139.67(7) 140.07(7)

Within the metallacycle **E**, two of the four tcm^- ligands act as ditopic linkers bridging two {$Cu_2(\mu_2$-$dppm)_2$} subunits with two terminal nitrile groups, with the remaining third nitrile group being uncoordinated and pointing outside of the assembly (Figure 1c). These two tcm^-

ligands are slightly bent out of the plane defined by the four Cu(I) ions (deviation of 0.611 Å) most probably to fit with the steric hindrance of the P-phenyl substituents of the dppm ligands that are orientated toward the center of the metallacycle (**Figure 1**c). The two others tcm^- ligands have a terminal ligand behavior and are only coordinated to the Cu1 center on side position (Figure 1c), pointing in opposite directions regarding the 'Cu_4' plane. The presence of these four tcm^- anions maintains the electro-neutrality of the supramolecular assembly. The Cu1 metal centers present a distorted P_2N_2 tetrahedral coordination sphere while the Cu2 centers have a P_2N_1 trigonal coordination sphere. The intermetallic Cu···Cu distance is slightly larger compared to the values observed in **B**, **C** and **D** derivatives (d(Cu-Cu) = 3.0948(5) Å for **E** being above the upper limit considered for cuprophilic interaction, Table 2).

These results illustrate the versatility of the supramolecular synthesis of metallacycles reacting U-shape molecular clip **A** with this series of pseudo-halide anions congeners, affording in total three cationic metallacycles (**B**, **C** and **D**) and a neutral species **E**. Surprisingly, in the latter case, the external monodentate tcm^- linkers do not lead to the formation of oligomeric or polymeric species, through a connection of the free 'C≡N' ligating moieties to a Cu(I) ion of an adjacent tetrametallic metallacycle. It is noteworthy that using an excess of clip **A**, only the metallacycle **E** is formed showing that the molecular clip **A** cannot coordinate the external pendant nitrile groups. Instead, networks of weak non-covalent interactions are formed between the hanging 'C≡N' branches of the external tcm^- and the phenyl rings and the methylene groups of the dppm ligands (Figure S37). One hypothesis to rationalize the selective formation of the neutral metallacycle **E** can be assigned to the shape and steric hindrance of the {$Cu_2(\mu_2$-dppm$)_2$} molecular subunits that cannot be coordinated on the scaffold of **E** due to the too short length of the pseudohalide linker tcm^-.

To explore further the formation of polymetallic assemblies based on the bimetallic subunits **A**, we have extended this study to the reaction of the ligands $\mathbf{L_1}$ and $\mathbf{L_2}$ (Scheme 1). These anionic

ligands have been selected for their four terminal nitrile functions that can lead to a tetratopic coordination mode, and have been reacted with **A**. Additionally, the ligands **L₁** and **L₂** were also reacted with the pre-assembled subunit **A'** {$Cu_2(\mu_2$-dppa$)_2$} to probe the impact of a slight variation in the structure of the diphosphane assembling ligand of the Cu(I) bimetallic units (dppm *versus* dppa ligand, the central –CH_2– methylene moiety lying between the phosphorus centers of the dppm ligand is formally replaced by a –NH– secondary amino group). The molecular-clip precursors **A** and **A'** formed in DCM solution were subsequently treated with half equivalent of **L1** or **L2** linkers dissolved in MeOH (Scheme 1). The resulting yellow mixtures were vigorously stirred overnight at room temperature and then left upon diethyl ether vapor diffusion, affording homogeneous polycrystalline batches after one-week. These reactions afforded after crystallization in good yields (80-90%) the species {[$Cu_2(\mu_2$-dppm$)_2$(**L$_m$**)PF_6]}$_n$ (**F** for m = 1 and **G** for m = 2), {[$Cu_2(\mu_2$-dppa$)_2$(**L₂**)PF_6]}$_n$ (**H**) and [$Cu_8(\mu_2$-dppa$)_8$(**L₁**)$_4(PF_6)_4$] (**I**) as light yellow polycrystalline powders (Scheme 1). The $^{31}P\{^1H\}$ NMR spectroscopic data in CD_2Cl_2 display broad singlet at - 9.13 ppm (**F**), - 9.89 ppm (**G**), 45.84 ppm (**H**), which are signals typical of the phosphorous atoms of dppm and dppa ligands in such Cu(I) dimers,[12–14,27] and reveal the formation of cationic Cu(I) species as typical PF_6^- anion signal is observed at *ca.* - 144 ppm (Figures S16-S18-S20). The cationic nature of these complexes is also confirmed by the presence of characteristic PF_6^- peak by solid-state IR analysis ($\upsilon(PF_6^-) \sim 835\ cm^{-1}$) that also reveals the presence of the anionic connecting ligands **L₁** and **L₂** in these derivatives (Figures S28-S29). The bimetallic subunits' scaffolds are preserved within these assemblies as supported by the room temperature ^1H NMR spectra (Figures S15-S17-S19)), in which no signals due to coordinated CH_3CN ligands are observed, and solid-state IR spectra suggest the presence of the **L₁** or **L₂** ligands.

Table 3. Crystallographic data of derivatives **F–I**

	F	**G**	**H**	**I**
Empirical formula	$C_{116}H_{93}ClCu_4F_{12}N_8P_{10}S_2$	$C_{59}H_{49}ClCu_2F_6N_4P_5S$	$C_{57}H_{47}ClCu_2F_6N_6P_5S$	$C_{224}H_{180}ClCu_8FN_{24}P_{16}S_4$
Formula weight (g.mol^{-1})	2454.96	1242.01	1244.00	4340.00
Temperature (K)	150(2)	150(2)	150(2)	150(2)
Crystal system	Triclinic	Monoclinic	Monoclinic	Orthorhombic
Space group	P-1	$P2_1/c$	$P2_1/n$	$I4_1/a$
a (Å)	14.763(2)	14.178(2)	16.796(1)	22.5260(4)
b (Å)	19.194(3)	34.848(4)	14.731(1)	22.526
*c (*Å)	22.667(4)	14.501(2)	26.421(2)	45.9578(12)
α (°)	88.665(5)	90	90	90
β (°)	84.394(5)	111.601(4)	95.757(2)	90
γ (°)	89.507(4)	90	90	90
V (Å^3)	6390.4(17)	6661.4(20)	6504.2(8)	23319.9(7)
Z	2	4	4	4
ρ_{calc} (g/cm^3)	1.276	1.238	1.270	1.236
μ (mm^{-1})	0.878	0.843	0.864	0.914
F(000)	2502.0	2536.0	2536.0	8912.0
Crystal size (mm^3)	0.21 × 0.08 × 0.06	0.25 × 0.07 × 0.06	0.25 × 0.11 × 0.08	0.23 × 0.19 × 0.07
Radiation	MoKα (λ = 0.71073)	MoKα (λ = 0.71069)	MoKα (λ = 0.71069)	MoKα (λ = 0.71069)
θ limit (°)	4.04 to 55.1	4.16 to 55.0	4.10 to 55.0	2.02 to 55.0
Index ranges *hkl*	$-18 \le h \le 19$ $-24 \le k \le 24$ $-29 \le l \le 29$	$-18 \le h \le 18$ $-45 \le k \le 40$ $-18 \le l \le 16$	$-21 \le h \le 21$ $-15 \le k \le 19$ $-34 \le l \le 34$	$-27 \le h \le 20$ $-14 \le k \le 29$ $-59 \le l \le 59$
Reflections collected	254018	68074	96134	53359
Independent reflections	29383	15276	14937	13371
Data/restraints/ parameters	29383/0/1339	15276/0/696	14937/0/686	13371/0/625
Goof on F^2	1.067	1.037	1.108	0.923
Final R[(a)] indexes [I≥2σ (I)] ωR[(b)] [I>2σ(I)]	R_1 = 0.1230 ωR_2 = 0.2423	R_1 = 0.0485 ωR_2 = 0.1047	R_1 = 0.0785 ωR_2 = 0.1408	R_1 = 0.0527 ωR_2 = 0.1360
Final R indexes (all data)	R_1 = 0.1811 ωR_2 = 0.2690	R_1 = 0.0714 ωR_2 = 0.1111	R_1 = 0.1041 ωR_2 = 0.1495	R_1 = 0.0872 ωR_2 = 0.1483
Largest diff. peak/hole (e.Å^{-3})	1.93/-0.95	0.77/-0.62	0.89/-0.93	0.59/-0.63
CCDC number	2305985	2305984	2305986	2305987

[(a)] $R = \Sigma||Fo|-|Fc||/\Sigma|Fo|$, [(b)] $\omega R = [\Sigma(\omega(Fo^2-Fc^2)^2)/\Sigma(\omega(Fo^2)^2)]^{1/2}$ with $\omega = 1/[(\sigma^2Fo^2)+(aP)^2+bP]$ and $P = (\max(Fo^2)+2Fc^2)/3$

The molecular structures of compounds **F-I** were determined thanks to single-crystal X-ray diffraction studies performed at 150 K (Table 3). Single crystals suitable for such analyses were obtained from diethyl ether vapor diffusions within CH_2Cl_2 solutions of each of these derivatives. In these derivatives, $\mathbf{L_1}$ and $\mathbf{L_2}$ ligands bridge the Cu(I) ions of the $\{Cu_2(\mu_2\text{-dppm})_2\}$ or $\{Cu_2(\mu_2\text{-dppa})_2\}$ fragments by two parallel 'C(CN)' branches involving two 'internal' CN moieties of the $\mathbf{L_1}$ and $\mathbf{L_2}$ ligands, to form a cyclic Cu–N–C_5–N–Cu moiety within $\{Cu_2(\mu_2\text{-dppm})_2\mathbf{L_m}\}$ subunits (**Figure 2** and 3). For **F**, **G** and **H**, two 'external' nitrile functions are coordinated to one Cu(I) ion of two different adjacent bimetallic subunits allowing, as a result of the self-assembly of these $\{Cu_2(\mu_2\text{-dppm})_2(\mathbf{L_m})\}$ fragments, the formation of supramolecular one-dimensional ladder-type polymeric assemblies (**Figure 2**). Conversely, in the derivative **I**, only one of the two 'external' nitrile group of the $\{Cu_2(\mu_2\text{-dppa})_2\mathbf{L_1}\}$ subunit is coordinated to one Cu(I) ion of an adjacent similar bimetallic fragment, leading to the formation of a octametallic metallacyclic cationic backbone adopting a twisted-square shape (Figure 3). One 'external' nitrile fragment for each of the four individual $\mathbf{L_1}$ ligand involved in the structure of **I** is left free from coordination and is pointing outside the assembly (Figure 3c).

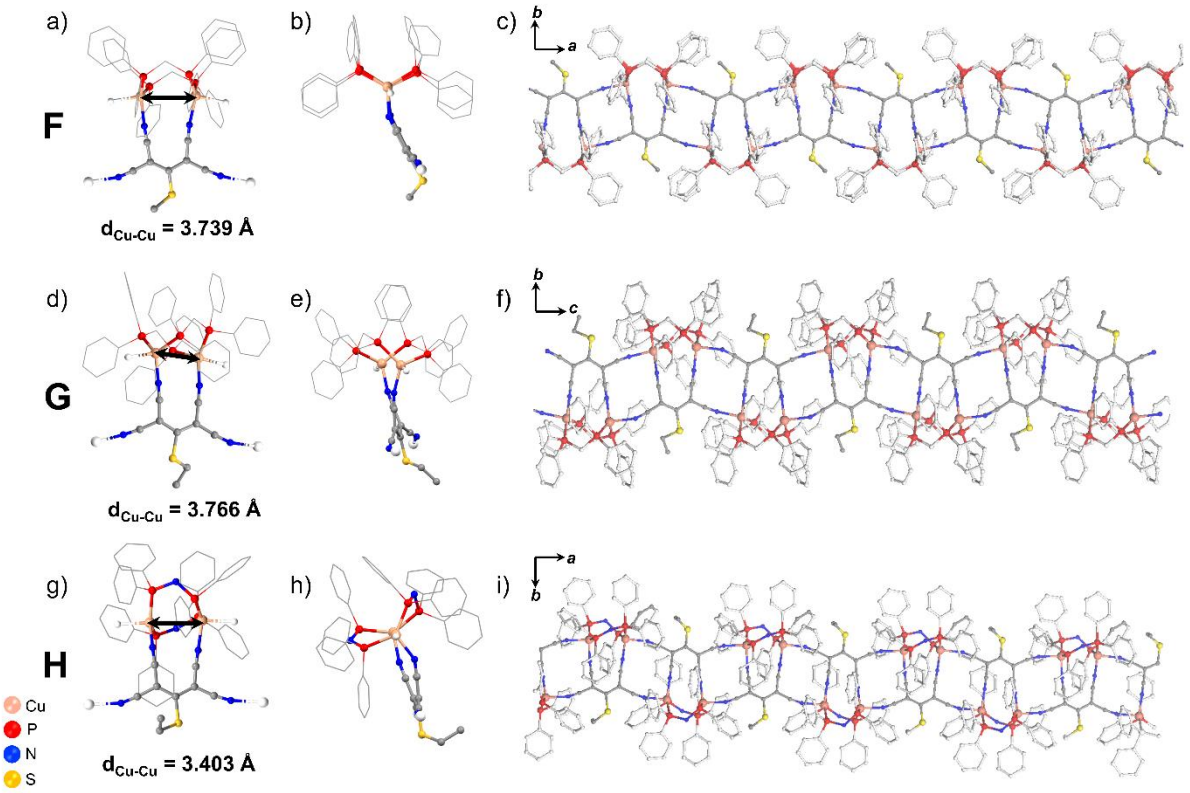

Figure 2. Molecular X-ray structures of derivatives **F**, **G** and **H:** 'Top' and 'side' views of the cyclic $[Cu_2(\mu_2\text{-dppm})_2L_m]^+$ (m = 1 or 2) and $[Cu_2(\mu_2\text{-dppa})_2L_2]^+$ subunits (a, d and g); side view (b, e and h); view of the 1D-ladder coordination polymers along their propagation axis (c, f and i). H atoms, counter-anions and included solvent molecules have been omitted for clarity.

Table 4. Selected bond lengths [Å] of the supramolecular assemblies **F–I**

	F	**G**	**H**	**I**
Cu–P	2.246(2), 2.283(2) 2.243(2), 2.265(2) 2.248(2), 2.253(2) 2.254(2), 2.272(2)	2.2701(8) 2.2581(9) 2.2592(9) 2.2829(9)	2.2498(12) 2.2664(12) 2.2485(13) 2.2687(13)	2.2718(10) 2.2960(10) 2.2063(10) 2.2327(11)
Cu–N	2.038(6), 2.080(6) 2.019(6), 2.088(7) 2.007(8), 2.072(7) 2.038(7), 2.122(7)	1.996(2) 2.125(2) 1.991(2) 2.192(2)	2.004(3) 2.097(4) 2.047(3) 2.106(4)	2.061(3) 2.112(3) 1.945(3)
Cu···Cu	3.739(1), 3.721(1)	3.766(1)	3.403(6)	2.929(8)

Note: In derivatives **G**, **H** and **I**, the two Cu(I) ions occupy two crystallographic independent sites and are denoted Cu1 and Cu2 (Figures S34-S35-S36). In compound **F**, the repeating unit contains two symmetrically independent $\{Cu_2(\mu_2\text{-dppm})_2(L1)\}^+$ fragments that are part of two different chains leading to four copper centers with different crystallographic environments (Cu1, Cu2, Cu3 and Cu4, Figure S33).

In the one-dimensional coordination polymers **F**, **G** and **H**, the coordination spheres of the Cu(I) ions adopt a P_2N_2 tetrahedral geometry occupied by two phosphorous atoms from dppm or dppa

ligands and two nitrogen atoms from **L₁** or **L₂** linkers. The orientation of these bimetallic units is alternated all along the propagation axis (Figure 2) inducing the ladder-like conformation to the one-dimensional coordination polymer. The coordination mode of the tetratopic **L₁** and **L₂** ligands increases the intermetallic distances Cu···Cu ranging in between 3.4035(7) – 3.7660(7) Å (Table 4) compared to the values observed in the series **B – E** (Table 2). The ladder-chains in the crystal packing are parallel to each other and separated by a layer of counter-anions that are weakly interacting with the phenyl rings of the dppm or dppa ligands.

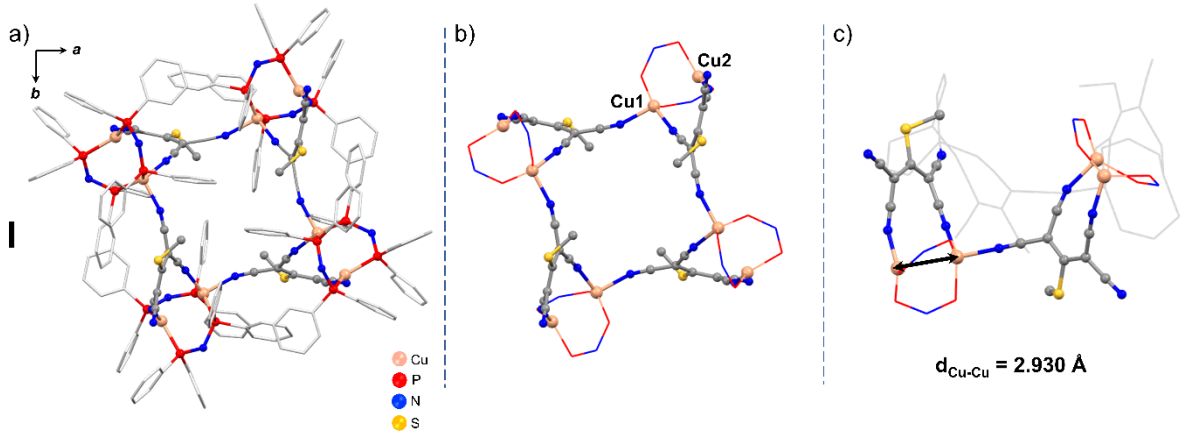

Figure 3. Molecular X-ray structure of derivative **I**. a) General view from the 'top' of the metallacycle and simplified views (phenyl rings have been omitted for clarity) from b) the 'top' and c) the side of the metallacycle.

In the octanuclear metallacycle **I**, Cu1 centers have a distorted P_2N_2 tetrahedral coordination sphere and Cu2 centers a trigonal P_2N_1 one and intermetallic distances (d(Cu-Cu) = 2.9297(9) Å) are shorter than those observed in the **F – H** derivatives (Table 4). The 'Cu_8' metallacyclic assembly can be described as adopting a '1,3-alternated'-like molecular structural conformation (Figure 3c). Importantly, in the crystal packing, each assembly is engaged in a H-bonds network connecting it with four neighboring molecules (Figure 4 and S38) *via* a double set of NH···N≡C interactions involving all pendant free 'external' nitrile fragment and one over the two NH moieties of each {$Cu_2(\mu_2$-dppa$)_2$} subunits. Interestingly, a PF_6^- counter-anion is found trapped inside the cavity generated inside the macrocyclic backbone (Figure 4c) while the other

remaining PF_6^- counter-anions are located between adjacent assemblies together with solvent molecules.

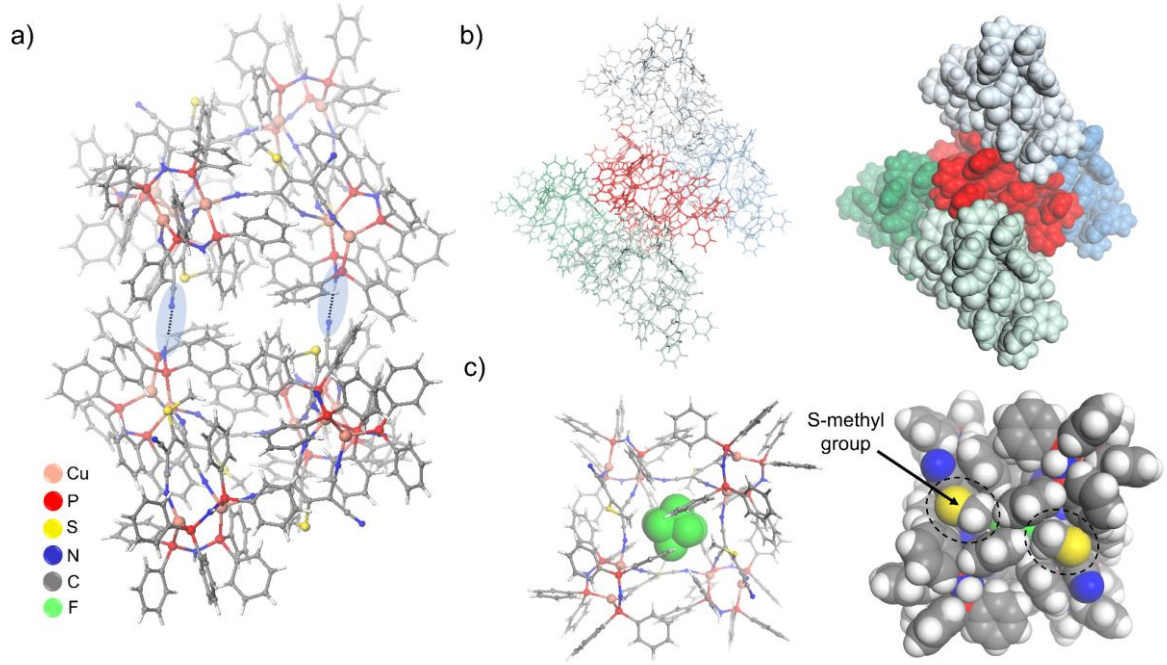

Figure 4. a) View of the H-bonds connecting locally two neighboring assemblies **I**; b) Stick and ball and CPK views of a central metallacycle (in red) and the four surrounding assemblies (blue, light blue, green and light green) involved in H-bonding interactions; c) Stick and ball and CPK views highlighting the PF_6^- counter-anion (light green) located in the cavity of the solid-state structure of derivative **I** and the optimal fit of the S-methyl group of **L1** in the volume available between the phenyl rings.

Therefore, reactions of the pre-assembled $\{Cu_2(\mu_2\text{-dppm})_2\}$ bimetallic fragment **A** with the series of anionic polytopic pseudohalide linkers (N_3^-, dca^- or tcm^-) and the $\mathbf{L_1}$ and $\mathbf{L_2}$ ligands afford selectively five new polymetallic assemblies **C**-**G**. In addition, the $\{Cu_2(\mu_2\text{-dppa})_2\}$ bimetallic precursor **A'** upon its reaction with the tetratopic $\mathbf{L_1}$ and $\mathbf{L_2}$ ligands allows obtaining two additional derivatives **H** and **I**. Together with the previous description of the tetrametallic compact metallacycle **B**, these syntheses confirmed the high ability of Cu(I) pre-assembled bimetallic precursors stabilized by $Ph_2P\text{-}X\text{-}PPh_2$ (X = CH_2, NH) diphosphine ligands to direct selective self-assembly reaction toward well-defined extended molecular scaffolds, in which the conformational flexibility of the Cu(I)-based precursors can tolerate significant alterations

such as intermetallic distances ranging from 2.867(1) Å (**B**)[12] up to 3.766(1) Å (**G**) while the coordination numbers of the two metal centers increase from 3:3 (**B** and **D**) to 3:4 (**C**, **E** and **I**) and finally to 4:4 (**F**, **G** and **H**).

Along this series of compounds, a large diversity in the dimensionalities and geometries of these assemblies is generated. Indeed, on the one hand, cationic tetrametallic derivatives **C** and **D** have global molecular scaffolds that compare the compact metallacycle framework observed in **B**.[12] On the other hand, the assembly **E** based on the tcm^- ligand exhibits a significantly different structure as an additional pseudo-halide ligand coordinates as monotopic terminal ligand one of the two Cu(I) metal centers, affording a neutral tetrametallic assembly. Compared to the CN^-, N_3^-, and dca^- fragments whose scaffolds' connectivity, in the first glance, is prone to promote their coordination as ditopic linkers, the tritopic molecular structure of the tcm^- anion might appear more suitable for the construction of higher nuclearity networks. However, CN^-, N_3^-, and dca^- ligands have been reported frequently to coordinate to more than two metal centers due to the formation of bridging coordination modes (as also observed for the N_3^- anion in the derivative **C**, Figure 1a) affording assemblies of high nuclearities. In addition, in the molecular backbone of **E**, the tcm^- ligands act either as ditopic linkers or terminal monotopic ligands. These observations suggest that the fate of the self-assembly processes conducted from the **A** precursor are mostly directed by the sterical constraints imposed by this building block regardless of the geometry and connectivity of the anionic pseudo-halides used. In our previous study,[28] the driving force leading to selective formation of compact tetrametallic metallacycles based on 'short' pseudohalide linkers was assigned to a 'sterical protection effect'. This effect relies on the shape and the steric hindrance of the bimetallic subunits $\{Cu_2(\mu_2\text{-dppm})_2\}$ that forbid subsequent interconnection of the metallacycle backbones through the coordination of an additional equivalent of linker due to sterical repulsion. According to the results described herein, such process very likely stands also for the reaction of the N_3^- and dca^- fragments with

the **A** precursor. However, as the tcm^- anion is reacted, one additional equivalent acting as monodentate terminal ligand is coordinated to one of the Cu(I) metal center of each bimetallic unit, but assembly of higher nuclearity cannot be isolated. Noteworthy, in a previous study, when longer neutral nitrile-capped linear ditopic π-conjugated linkers were reacted with the fragment **A**, 1D-coordination polymers were obtained, alternating related tetrametallic metallacycles connected by the linkers used.[29] This supports the assumption of a dependance of the dimensionality of the networks formed with the length of the linkers.

In line with these observations and assumptions, as the longer tetradentate ligands $\mathbf{L_1}$ and $\mathbf{L_2}$ are reacted with the pre-assembled **A** subunit, polymeric assemblies **F** and **G** were obtained, which have higher dimensionality than the discrete derivatives **B-E**. Their molecular architectures are significantly different, as compact tetrametallic metallacycles are no longer observed. However, one can note that within the extended one-dimensional frameworks of **F** and **G**, there is the formation instead of analogous cyclic Cu–N–C_5–N–Cu units. Interestingly, as the $\{Cu_2(\mu_2\text{-dppa})_2\}$ bimetallic precursor **A'** is reacted with the tetradentate $\mathbf{L_2}$ ligand, the one-dimensional coordination polymer **H** is obtained (**Figure 2**c) bearing the same molecular architecture than the equivalent dppm-based one-dimensional coordination polymer **G** (**Figure 2**b). Conversely, when the tetradentate $\mathbf{L_1}$ ligand is reacted with **A**', a discrete octametallic metallacyclic structure is isolated that is markedly different from the one-dimensional coordination polymer **F**. Such a discrepancy highlights how subtle changes in the backbone of the building-block introduced in these self-assembly reactions can have major impact on the resulting molecular structures. Indeed, the tetradentate $\mathbf{L_1}$ and $\mathbf{L_2}$ ligands only differ by the nature of the aliphatic groups carried by the central pendant S-atom ($\mathbf{L_1}$: methyl *versus* $\mathbf{L_2}$: ethyl, Scheme 1) which do not impact the fate of the self-assembly processes taking place as these ligands are reacted with bimetallic precursor **A**. However, with the dppa ligand, intermolecular H-bonds are generated between the isolated discrete assemblies of **I** bearing the

L_1 ligand but do not appear in the one-dimensional coordination polymer **H** bearing the **L_2** ligand. As it can be seen in the **Figure 4**c, the S-methyl group of the **L_1** ligand in the molecular structure of **I** optimally fit the volume available over the internal cavity that contains the encapsulated PF_6^- anion. This would not be possible with the bulkier S-ethyl group of the **L_2** ligand which very likely disfavors in this case the formation of an octametallic metallacycle to the benefit of the formation of 1D ladder structures observed. Moreover, the formation of derivative **I** is also promoted by the formation of the intermolecular H-bond network involving the pendant free 'external' nitrile fragments of the **L_1** ligand and the NH fragment of the dppa ligand and the encapsulated PF_6^- counter-anion, weak cumulated stabilizing contributions that cannot take place with the precursor **A** based on the dppm ligand.

Photophysical properties:

The tetrametallic metallacycle **B** is an efficient TADF luminophore (quantum yield of 72 %) which emits an eye-perceived intense blue light in the solid state at RT upon photoexcitation.[12] The related tetrametallic metallacyclic structure adopted by derivatives **C**, **D** and **E** encouraged us to investigate their photophysical properties in solid-state. The crystals of these derivatives are colorless under visible light and they display under UV irradiation (λ_{ex} = 365 nm) very weak yellowish (**C** and **E**) and greenish (**D**) eye-perceived emissions at RT and at 80 K in solid-state. Absorption spectra at room temperature of these derivatives show a broad band in the near UV-region centered at 332 nm (**C**), 316 nm (**D**) and 288 nm (**E**), typical of MLCT transitions[12] (Figure S39). No absorption is observed in the visible region of these spectra which is in agreement with the colorless aspect of the polycrystalline powder samples obtained. These derivatives are characterized with a very weak RT intensity of emitted light in the solid state upon photoexcitation that precludes conducting systematic extensive variable-temperature (VT) studies of their photophysical properties in order to highlight the radiative relaxation processes taking place. Therefore, only the low temperature properties are reported herein for

derivatives **C** and **E**. The excitation spectra at 80 K of these three derivatives show large excitation domain in the near UV region with one maximum and one shoulder for each compound respectively (**Figure 5**a). Upon excitation at 398 nm (**C**), 324 nm (**D**) and 362 nm (**E**) at 80 K, polycrystalline batches of these three compounds exhibit broad and featureless emission bands characterized by λ_{max} = 540 nm (**C**), 489 nm (**D**) and 522 nm (**E**) (**Figure 5**a) with biexponential decay times of 205 µs and 45 µs for **C** and 233 µs and 71 µs for **E**, and with monoexponential decay time of 198 µs for **D** (Table 5).

Table 5. Photophysical data for derivatives **B–I** in solid-state.

	λ_{ex} (nm)	λ_{em}^{80K} (nm)	λ_{em}^{300K} (nm)	τ^{80K} (ms)
B[12]	320	486	457	0.200 0.040
C	398	540	–	0.205 0.045
D	324	489	475	0.198
E	362	522	–	0.233 0.071
F	420	595	492	7.6 4.3
G	440	555	502	11 20
H	440	554	500	10 3.5
I	408	506	483	9.2 5.9

The temperature dependent emission behavior of derivative **C** was investigated only between 80-150 K (at higher temperature the intensity of the signal was too weak to be measured, Figure **5**S42). The emission intensity smoothly increases upon cooling down the temperature with no variation of the wavelength of the emission maximum. The temperature dependent emission behavior of derivative **D** was studied between 80 K and 300 K. It shows a decrease of intensity upon heating up the sample from 80 K to room temperature (Figure S42) associated with a slight blueshift of the emission maximum (Figure 5b) which is centered at 475 nm at 300 K.

The thermal-variation of its decay time was studied from 80 K to 260 K. It decreases progressively from 80 K to 180 K and then abruptly drops down to reach 9 µs at 260 K (Figure 5c). The thermochromic emission behavior and the sigmoidal profile afforded by the VT lifetime decay are typical of a TADF radiative relaxation process.[18] Tentatively, by fitting the VT decay time to Eq (S1) in the ESI, the values of $\Delta E(S_1–T_1)$ = 1371 cm^{-1}, $\tau(T_1)$ = 192 µs and $\tau(S_1)$ = 3.6 ns could be obtained (Figure S42). However, since it was not possible to reach a plateau in the high temperature regime (above 260 K) for the measurements of the decay time due to the weakness of the signal, the values obtained from this fit should be considered with caution.

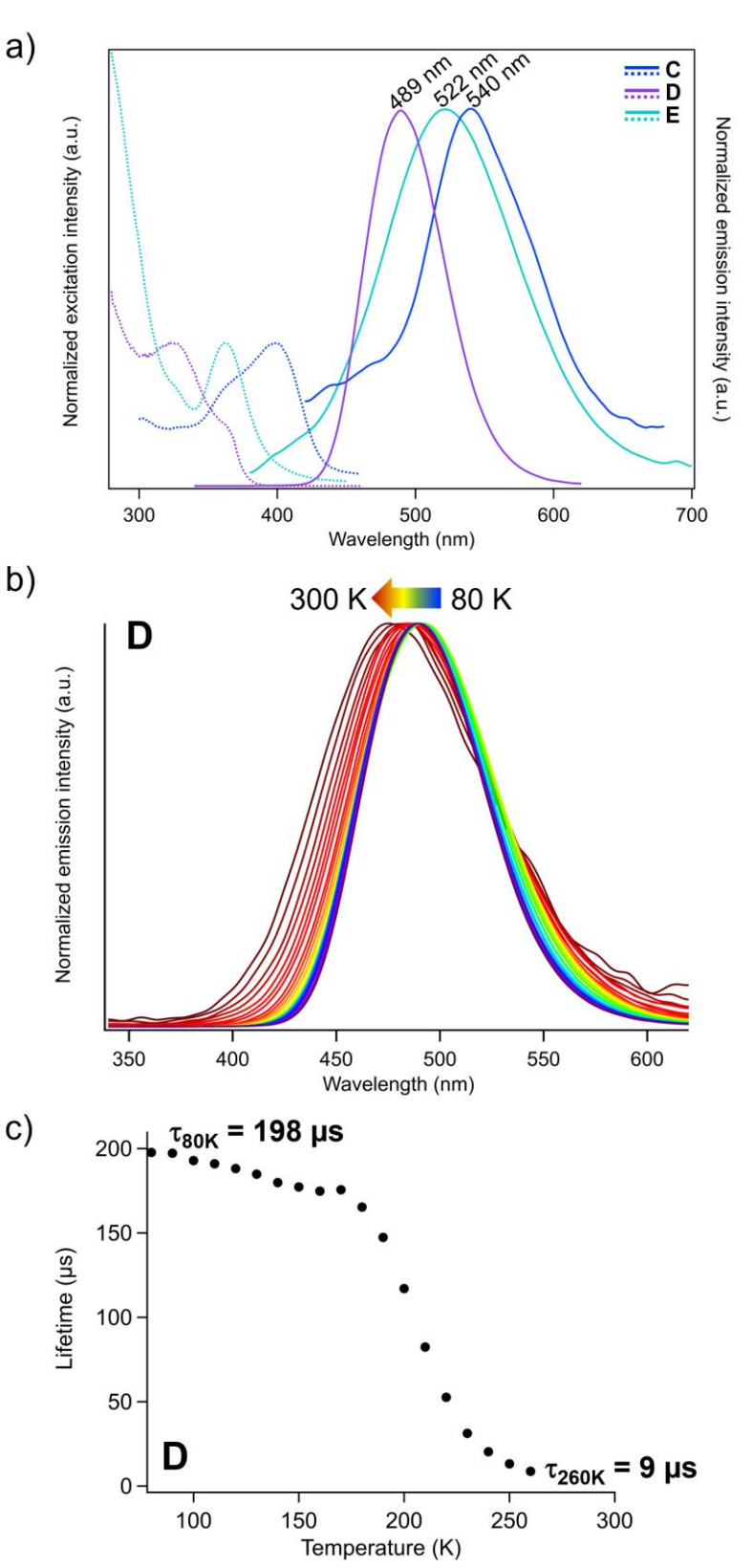

Figure 5. a) Excitation spectra (doted lines) and emission spectra (bold lines) of derivatives **C** (λ_{ex} = 398 nm), **D** (λ_{ex} = 324 nm) and **E** (λ_{ex} = 362 nm) at 80 K in solid-state. b) Temperature-dependent normalized emission spectra of derivative **D** upon excitation at 324 nm in solid state. c) Decay-time temperature variation of derivative **D** upon excitation at 330 nm.

The crystals of derivatives **F**, **G**, **H** and **I** are yellow colored under visible light and they display an eye-perceived yellowish emission in solid-state at RT under UV irradiation (λ_{ex} = 365 nm). The UV–visible absorption spectra of these derivatives (Figures S40-S41) present broad bands centered at 396 nm for **F** and **G**, at 382 nm with a shoulder at *ca.* 416 nm for **H**, and at 376 nm with a shoulder at *ca.* 434 nm for **I**. These bands are assigned to typical MLCT transitions.[12] Absorption spectra display also some signal intensity in the visible region which is in agreement with the yellow color of the polycrystalline powder samples obtained. Upon excitation at 420 nm (**F**), 440 nm (**G** and **H**) and 408 nm (**I**) at 300 K (see excitation spectra Figure S43), their emission spectra exhibit a large and asymmetrical band centered at 492 nm (**F**), 502 nm (**G**), 500 nm (**H**) and 483 nm (**I**) suggesting HE/LE mixed-emission (HE: high energy; LE: low energy). Upon cooling from 300 to 80 K, a gradual drop of intensity of these HE bands along with an appearance of a low energy bands (LE) is observed affording at 80 K LE emission maxima centered at 595 nm, 555 nm, 554 nm and 506 nm for **F**, **G**, **H** and **I** respectively (Figure 6). The decay times were determined focusing on the emission of the LE excited state, while the lifetime of the HE bands revealed to reach value of the nanosecond order, which is above the measuring threshold set-up. These emission decay times were treated by biexponential fits affording at 80 K τ_1 and τ_2 of millisecond order (7.6 ms and 4.3 ms (**F**), 11 ms and 2.0 ms (**G**), 9.2 ms and 5.9 ms (**H**), 10 ms and 3.5 ms (**I**), **Figure 6** and Table 5). The temperature-dependent variation decay time profiles (depending of the derivatives, measurements of the decay time could not be performed at higher temperatures due to the weakness of the signal) show a progressive decrease upon heating up and the lifetimes reach 26 µs and 1 µs at 300 K for **F**, 3.3 ms and 0.39 ms at 160 K for **G**, 2.0 ms and 0.46 ms at 170 K for **H** and 0.89 ms and 0.28 ms at 250 K for **I** (**Figure 6** and Table 5).

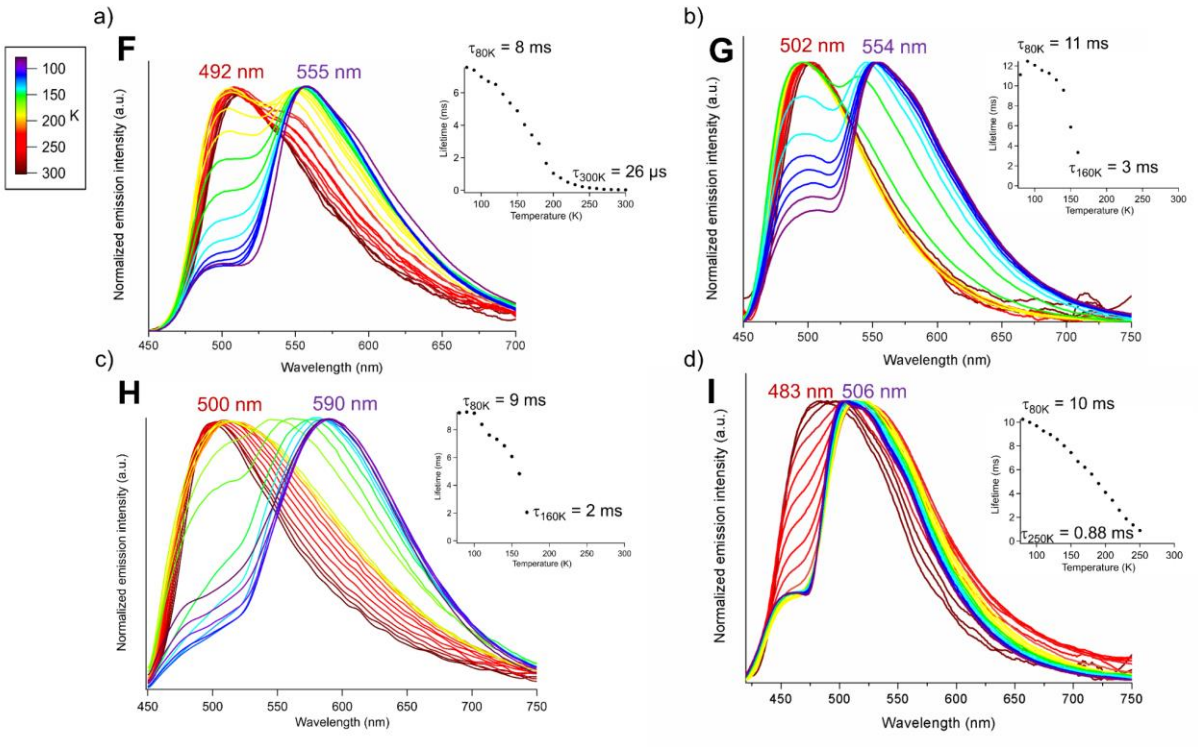

Figure 6. Emission spectra at variable temperature of derivatives **F** (λ_{ex} = 420 nm (a)), **G** (λ_{ex} = 440 nm (b)), **H** (λ_{ex} = 440 nm (c)) and **I** (λ_{ex} = 408 nm (d)) together with their temperature dependent decay time variation upon excitation at 404 nm.

The solid-state luminescence study for these derivatives **F**-**I** confirms the presence of thermochromic behaviors in these systems, even though the spectral shifts are very moderate (Figure 6). This clearly suggests temperature-dependent competitive relaxation processes with very likely $\mathbf{L_m}$ (m = 1, 2) metal-perturbed ligand centered fluorescence of the HE bands observed in the high temperature regime and ^{3}MLCT phosphorescence centered on the bimetallic $\{Cu_2(\mu_2\text{-dppx})_2\}$ (x = m, a) subunits for the LE bands observed in the low temperature domain. However, a thorough understanding of the origin of these emission behaviors cannot be provided by these experimental measurements and would benefit extended TD-DFT calculations. Yet, the large size of these assemblies, the influence of the solid-state packing on their geometries[12,14,17] and the weak RT photoluminescence intensities they exhibit did not trigger us to perform full DFT geometry optimization of their excited states to get deep

insights about the electronic causes of these different photophysical properties. Likely, the very moderate photoluminescence properties recorded at RT in the solid-state for the new derivatives **C**-**I**[30] are due to efficient non-radiative relaxation processes associated with vibrational modes carried by the ligating moieties of the linkers used. Indeed, it is worth to note that the typical infrared bands of the pseudo-halide ligands in the infrared spectra of derivatives **C**-**I** (Figure S25-S29) present intensities that are much stronger than the band observed for the C≡N stretching of the cyano ligand in the reference compound **B**.[12] This very likely indicates vibrational modes that are much more active for the anionic ligands in the series of derivatives **C**-**I** than in the compound **B** and corelate with the much more intense emission properties of the latter. Indeed, in the case of derivatives **C**-I, very efficient non-radiative relaxation pathways due to the vibrations lying on the connecting ligands are likely taking place which results in a weakening of the emission efficiencies of these compounds (in addition, cuprophilic are also much more intense in derivative **B**[12] than in any compound of the series **C**-**I** which also very likely is another parameter that promotes more efficient radiative relaxation processes in derivative **B**[12]). However, all in all, the photophysical properties exhibited by the series of compounds **C**-**I** are coherent regarding those recently reported in the case of RT moderately luminescent Cu(I) assemblies ranging from TADF[18] in the case of the derivative **D** to phosphorescence in the case of the other compounds **C, E**-**I**.[12–15,20–23,26,27,31–51]

CONCLUSION

The ability of bimetallic molecular clips **A** and **A'** to assemble through polytopic linkers selectively within supramolecular metallacycles or coordination polymers is confirmed with this study. The selective formation of the tetrametallic metallacycle backbones observed in the derivatives **C**, **D** and **E** using the 'short' pseudohalide linkers N_3^-, dca^- and tcm^- could be assigned to a 'sterical protection effect' resulting from the large steric hindrance and specific shape of the bimetallic fragments. In contrast, larger bridging ligands $\mathbf{L_1}$ and $\mathbf{L_2}$ formed

supramolecular assemblies having higher nuclearity and dimensionality with **A** and **A'**, whose scaffolds differ from those of the tetrametallic subunits observed in the derivatives **B**[12]**-E**. These results reveal how the steric hindrance of the Cu(I) bimetallic precursors (**A** or **A'**), the properties eventually carried by the diphosphine dppm or dppa ligands (such as a possibility of H-bonding) and the dimension of the anionic ligands can play a crucial role toward the formation of polymetallic Cu(I)-assemblies characterize by specific backbones. All these derivatives, conversely to the derivative **B**,[12] present weakly intense RT solid-state photoemission properties. However, regarding the various luminescent multifunctional derivatives that have been obtained so far from the tetrametallic metallacycle **B** (Scheme 2), a strong interest should be devoted in the future in conducting analogous studies of the reactivity of the assemblies **C**-**I**.

ASSOCIATED CONTENT

SUPPORTING INFORMATION

The Supporting Information is available free of charge at https://pubs.acs.org/doi/xxxxx.

Details on materials and experimental instruments; synthesis procedures NMR spectra; FTIR spectra; X-ray crystallography; thermal ellipsoid and photophysical studies (PDF).

CCDC 2305984−2305987 and 2305989-2305991 contain the supplementary crystallographic data for this paper. These data can be obtained free of charge via www.ccdc.cam.ac.uk/data_request/cif, or by emailing data_request@ccdc.cam.ac.uk, or by contacting The Cambridge Crystallographic Data Centre, 12 Union Road, Cambridge CB2 1EZ, UK; fax: +44 1223 336033.

Notes

The authors declare no competing financial interest.

ACKNOWLEDGMENTS

This work was supported by the CNRS, l'Agence nationale de la recherche (ANR PRC SMAC, ANR PRCI SUPRALUM and ANR PRC Mol-CoSM Projects), the French 'Ministère de l'Enseignement Supérieur, de la Recherche et de l'Innovation' and the French 'Ministère des Affaires Etrangères'. C.X. acknowledge the Chinese Scholarship Council for a doctoral scholarship.

REFERENCES

(1) Vantomme, G.; Meijer, E. W. The Construction of Supramolecular Systems. *Science* **2019**, *363* (6434), 1396–1397. https://doi.org/10.1126/science.aav4677.
(2) Cook, T. R.; Stang, P. J. Recent Developments in the Preparation and Chemistry of Metallacycles and Metallacages via Coordination. *Chem. Rev.* **2015**, *115* (15), 7001–7045. https://doi.org/10.1021/cr5005666.
(3) Harris, K.; Fujita, D.; Fujita, M. Giant Hollow MnL2n Spherical Complexes: Structure, Functionalisation and Applications. *Chem. Commun.* **2013**, *49* (60), 6703–6712. https://doi.org/10.1039/C3CC43191F.
(4) Wang, W.; Wang, Y.-X.; Yang, H.-B. Supramolecular Transformations within Discrete Coordination-Driven Supramolecular Architectures. *Chem. Soc. Rev.* **2016**, *45* (9), 2656–2693. https://doi.org/10.1039/C5CS00301F.
(5) Fujita, M.; Tominaga, M.; Hori, A.; Therrien, B. Coordination Assemblies from a Pd(II)-Cornered Square Complex. *Acc. Chem. Res.* **2005**, *38* (4), 369–378. https://doi.org/10.1021/ar040153h.
(6) Pullen, S.; Clever, G. H. Mixed-Ligand Metal–Organic Frameworks and Heteroleptic Coordination Cages as Multifunctional Scaffolds—A Comparison. *Acc. Chem. Res.* **2018**, *51* (12), 3052–3064. https://doi.org/10.1021/acs.accounts.8b00415.
(7) Bardhan, D.; Chand, D. K. Palladium(II)-Based Self-Assembled Heteroleptic Coordination Architectures: A Growing Family. *Chem. Eur. J.* **2019**, *25* (53), 12241–12269. https://doi.org/10.1002/chem.201900831.
(8) Sinha, N.; Hahn, F. E. Metallosupramolecular Architectures Obtained from Poly-N-Heterocyclic Carbene Ligands. *Acc. Chem. Res.* **2017**, *50* (9), 2167–2184. https://doi.org/10.1021/acs.accounts.7b00158.
(9) Dong, J.; Pan, Y.; Wang, H.; Yang, K.; Liu, L.; Qiao, Z.; Yuan, Y. D.; Peh, S. B.; Zhang, J.; Shi, L.; Liang, H.; Han, Y.; Li, X.; Jiang, J.; Liu, B.; Zhao, D. Self-Assembly of Highly Stable Zirconium(IV) Coordination Cages with Aggregation Induced Emission Molecular

Rotors for Live-Cell Imaging. *Angew. Chem. Int. Ed.* **2020**, *59* (25), 10151–10159. https://doi.org/10.1002/anie.201915199.
(10) Schiller, J.; Peresypkina, E.; Virovets, A. V.; Scheer, M. Metal-Deficient Supramolecule Based on a Fivefold-Symmetric Building Block. *Angew. Chem. Int. Ed.* **2020**, *59* (32), 13647–13650. https://doi.org/10.1002/anie.202004988.
(11) Lescop, C. Coordination-Driven Supramolecular Synthesis Based on Bimetallic Cu(I) Precursors: Adaptive Behavior and Luminescence. *Chem. Rec.* **2021**, *21* (3), 544–557. https://doi.org/10.1002/tcr.202000144.
(12) El Sayed Moussa, M.; Evariste, S.; Wong, H.-L.; Le Bras, L.; Roiland, C.; Le Polles, L.; Le Guennic, B.; Costuas, K.; Yam, V. W.-W.; Lescop, C. A Solid State Highly Emissive Cu(I) Metallacycle: Promotion of Cuprophilic Interactions at the Excited States. *Chem. Commun.* **2016**, *52* (76), 11370–11373. https://doi.org/10.1039/C6CC06613E.
(13) Evariste, S.; Khalil, A. M.; Moussa, M. E.; Chan, A. K.-W.; Hong, E. Y.-H.; Wong, H.-L.; Le Guennic, B.; Calvez, G.; Costuas, K.; Yam, V. W.-W.; Lescop, C. Adaptive Coordination-Driven Supramolecular Syntheses toward New Polymetallic Cu(I) Luminescent Assemblies. *J. Am. Chem. Soc.* **2018**, *140* (39), 12521–12526. https://doi.org/10.1021/jacs.8b06901.
(14) El Sayed Moussa, M.; Khalil, A. M.; Evariste, S.; Wong, H.-L.; Delmas, V.; Guennic, B. L.; Calvez, G.; Costuas, K.; Yam, V. W.-W.; Lescop, C. Intramolecular Rearrangements Guided by Adaptive Coordination-Driven Reactions toward Highly Luminescent Polynuclear Cu(I) Assemblies. *Inorg. Chem. Front.* **2020**, *7* (6), 1334–1344. https://doi.org/10.1039/C9QI01595G.
(15) Evariste, S.; Xu, C.; Calvez, G.; Lescop, C. Straightforward Coordination-Driven Supramolecular Chemistry Preparation of a Discrete Solid-State Luminescent Cu4 Polymetallic Compact Assembly Based on Conformationally Flexible Building Blocks. *Inorg. Chim. Acta* **2021**, *516*, 120115. https://doi.org/10.1016/j.ica.2020.120115.
(16) Harisomayajula, N. V. S.; Makovetskyi, S.; Tsai, Y.-C. Cuprophilic Interactions in and between Molecular Entities. *Chem. Eur. J.* **2019**, *25* (38), 8936–8954. https://doi.org/10.1002/chem.201900332.
(17) Moutier, F.; Schiller, J.; Lecourt, C.; Khalil, A. M.; Delmas, V.; Calvez, G.; Costuas, K.; Lescop, C. Impact of Intermolecular Non-Covalent Interactions in a CuI8PdII1 Discrete Assembly: Conformers' Geometries and Stimuli-Sensitive Luminescence Properties. *Chem. Eur. J.* **2022**, *28* (24), e202104497. https://doi.org/10.1002/chem.202104497.
(18) *Highly Efficient OLEDs: Materials Based on Thermally Activated Delayed Fluorescence*, 1st ed.; Yersin, H., Ed.; Wiley, 2018. https://doi.org/10.1002/9783527691722.
(19) Czerwieniec, R.; Leitl, M. J.; Homeier, H. H. H.; Yersin, H. Cu(I) Complexes – Thermally Activated Delayed Fluorescence. Photophysical Approach and Material Design. *Coord. Chem. Rev.* **2016**, *325*, 2–28. https://doi.org/10.1016/j.ccr.2016.06.016.
(20) Kobayashi, A.; Kato, M. Stimuli-Responsive Luminescent Copper(I) Complexes for Intelligent Emissive Devices. *Chem. Lett.* **2017**, *46* (2), 154–162. https://doi.org/10.1246/cl.160794.
(21) Hupp, B.; Nitsch, J.; Schmitt, T.; Bertermann, R.; Edkins, K.; Hirsch, F.; Fischer, I.; Auth, M.; Sperlich, A.; Steffen, A. Stimulus-Triggered Formation of an Anion–Cation Exciplex in Copper(I) Complexes as a Mechanism for Mechanochromic Phosphorescence. *Angew. Chem. Int. Ed.* **2018**, *57* (41), 13671–13675. https://doi.org/10.1002/anie.201807768.
(22) Artem'ev, A. V.; Pritchina, E. A.; Rakhmanova, M. I.; Gritsan, N. P.; Bagryanskaya, I. Y; Malysheva, S. F.; Belogorlova, N. A. Alkyl-Dependent Self-Assembly of the First Red-Emitting Zwitterionic {Cu 4 I 6 } Clusters from [Alkyl-P(2-Py) 3] + Salts and CuI: When Size Matters. *Dalton Trans.* **2019**, *48* (7), 2328–2337. https://doi.org/10.1039/C8DT04328K.

(23) Chakkaradhari, G.; Eskelinen, T.; Degbe, C.; Belyaev, A.; Melnikov, A. S.; Grachova, E. V.; Tunik, S. P.; Hirva, P.; Koshevoy, I. O. Oligophosphine-Thiocyanate Copper(I) and Silver(I) Complexes and Their Borane Derivatives Showing Delayed Fluorescence. *Inorg. Chem.* **2019**, *58* (6), 3646–3660. https://doi.org/10.1021/acs.inorgchem.8b03166.
(24) Hamze, R.; Peltier, J. L.; Sylvinson, D.; Jung, M.; Cardenas, J.; Haiges, R.; Soleilhavoup, M.; Jazzar, R.; Djurovich, P. I.; Bertrand, G.; Thompson, M. E. Eliminating Nonradiative Decay in Cu(I) Emitters: >99% Quantum Efficiency and Microsecond Lifetime. *Science* **2019**, *363* (6427), 601–606. https://doi.org/10.1126/science.aav2865.
(25) Lescop, C. Coordination-Driven Syntheses of Compact Supramolecular Metallacycles toward Extended Metallo-Organic Stacked Supramolecular Assemblies. *Acc. Chem. Res.* **2017**, *50* (4), 885–894. https://doi.org/10.1021/acs.accounts.6b00624.
(26) Naik, S.; Mague, J. T.; Balakrishna, M. S. Short-Bite PNP Ligand-Supported Rare Tetranuclear [Cu4I4] Clusters: Structural and Photoluminescence Studies. *Inorg. Chem.* **2014**, *53* (7), 3864–3873. https://doi.org/10.1021/ic500240j.
(27) Moutier, F.; M. Khalil, A.; A. Baudron, S.; Lescop, C. Gleaned Snapshots on the Road to Coordination Polymers: Heterometallic Architectures Based on Cu(i) Metallaclips and 2,2′-Bis-Dipyrrin Metalloligands. *Chem. Commun.* **2020**, *56* (72), 10501–10504. https://doi.org/10.1039/D0CC04862C.
(28) Vreshch, V.; Nohra, B.; Lescop, C.; Réau, R. Synthesis of Small Tetranuclear Cu(I) Metallacycles Based on Bridging Pseudohalogenide Ions. *Inorg. Chem.* **2013**, *52* (3), 1496–1503. https://doi.org/10.1021/ic3022535.
(29) Nohra, B.; Yao, Y.; Lescop, C.; Réau, R. Coordination Polymers with π-Stacked Metalloparacyclophane Motifs: F-Shaped Mixed-Coordination Dinuclear Connectors. *Angew. Chem. Int. Ed.* **2007**, *46* (43), 8242–8245. https://doi.org/10.1002/anie.200702756.
(30) Derivatives **C**-**I** present in the solid-state very moderate eye-perceived light emission in terms of intensity. It is only as the compounds are cooled that this emission gains a significant intensity. Unfortunately, our local set-up only allows the measurements of RT emission quantum yields and even with the apparently more emissive'' compounds of the series, the determination of these emission quantum yields was highly non reproductible, yet very weak (ca. below 5 %), very likely as a result of both very low intensity absorption and emission spectra.
(31) Belyaev, A.; Eskelinen, T.; Dau, T. M.; Ershova, Y. Yu.; Tunik, S. P.; Melnikov, A. S.; Hirva, P.; Koshevoy, I. O. Cyanide-Assembled d ^{10} Coordination Polymers and Cycles: Excited State Metallophilic Modulation of Solid-State Luminescence. *Chemistry A European J* **2018**, *24* (6), 1404–1415. https://doi.org/10.1002/chem.201704642.
(32) Gusev, A.; Kiskin, M.; Braga, E.; Zamnius, E.; Kryukova, M.; Karaush-Karmazin, N.; Baryshnikov, G.; Minaev, B.; Linert, W. Structure and Emission Properties of Dinuclear Copper (i) Complexes with Pyridyltriazole. *RSC advances* **2023**, *13* (6), 3899–3909.
(33) Jaros, S. W.; Sokolnicki, J.; Siczek, M.; Smoleński, P. Strategy for an Effective Eco-Optimized Design of Heteroleptic Cu(I) Coordination Polymers Exhibiting Thermally Activated Delayed Fluorescence. *Inorg. Chem.* **2023**, *62* (49), 19898–19907. https://doi.org/10.1021/acs.inorgchem.3c01908.
(34) Kikuchi, K.; Imoto, H.; Naka, K. Robust and Highly Emissive Copper (i) Halide 1D-Coordination Polymers with Triphenylarsine and a Series of Bridging N-Heteroaromatic Co-Ligands. *Dalton Transactions* **2023**, *52* (32), 11168–11175.
(35) Paderina, A.; Melnikov, A.; Slavova, S.; Sizov, V.; Gurzhiy, V.; Petrovskii, S.; Luginin, M.; Levin, O.; Koshevoy, I.; Grachova, E. The Tail Wags the Dog: The Far Periphery of the Coordination Environment Manipulates the Photophysical Properties of Heteroleptic Cu (I) Complexes. *Molecules* **2022**, *27* (7), 2250.

(36) Schlachter, A.; Scheel, R.; Fortin, D.; Strohmann, C.; Knorr, M.; Harvey, P. D. Chain Length Effect on the Structural and Emission Properties of the CuI/Bis((4-Methoxyphenyl)Thio)Alkane Coordination Polymers. *Inorg. Chem.* **2022**, *61* (29), 11306–11318. https://doi.org/10.1021/acs.inorgchem.2c01427.
(37) Schlachter, A.; Tanner, K.; Scheel, R.; Karsenti, P.-L.; Strohmann, C.; Knorr, M.; Harvey, P. D. A Fused Poly(Truncated Rhombic Dodecahedron)-Containing 3D Coordination Polymer: A Multifunctional Material with Exceptional Properties. *Inorg. Chem.* **2021**, *60* (17), 13528–13538. https://doi.org/10.1021/acs.inorgchem.1c01856.
(38) Schlachter, A.; Viau, L.; Fortin, D.; Knauer, L.; Strohmann, C.; Knorr, M.; Harvey, P. D. Control of Structures and Emission Properties of $(CuI)_n$ 2-Methyldithiane Coordination Polymers. *Inorg. Chem.* **2018**, *57* (21), 13564–13576. https://doi.org/10.1021/acs.inorgchem.8b02168.
(39) Zhang, R.; Liu, J.-W.; Zhong, W.-Y.; Chen, J.-L.; Zhao, F.; Liu, S.-J.; Wen, H.-R. Mechanochromic and Selective Vapochromic Solid-State Luminescence of a Dinuclear Cuprous Complex. *Inorg. Chem.* **2023**, *62* (29), 11510–11517. https://doi.org/10.1021/acs.inorgchem.3c01107.
(40) Schlachter, A.; Harvey, P. D. Properties and Applications of Copper Halide-Chalcogenoether and -Chalcogenone Networks and Functional Materials. *J. Mater. Chem. C* **2021**, *9* (21), 6648–6685. https://doi.org/10.1039/D1TC00585E.
(41) Strelnik, I.; Shamsieva, A.; Akhmadgaleev, K.; Gerasimova, T.; Dayanova, I.; Kolesnikov, I.; Fayzullin, R.; Islamov, D.; Musina, E.; Karasik, A.; Sinyashin, O. Emission and Luminescent Vapochromism Control of Octahedral Cu4I4 Complexes by Conformationally Restricted P,N Ligands. *Chemistry – A European Journal* **2023**, *29* (10), e202202864. https://doi.org/10.1002/chem.202202864.
(42) Kobayashi, A.; Yoshida, Y.; Yoshida, M.; Kato, M. Mechanochromic Switching between Delayed Fluorescence and Phosphorescence of Luminescent Coordination Polymers Composed of Dinuclear Copper(I) Iodide Rhombic Cores. *Chemistry – A European Journal* **2018**, *24* (55), 14750–14759. https://doi.org/10.1002/chem.201802532.
(43) Hayashi, T.; Kobayashi, A.; Ohara, H.; Yoshida, M.; Matsumoto, T.; Chang, H.-C.; Kato, M. Vapochromic Luminescence and Flexibility Control of Porous Coordination Polymers by Substitution of Luminescent Multinuclear Cu(I) Cluster Nodes. *Inorg. Chem.* **2015**, *54* (18), 8905–8913. https://doi.org/10.1021/acs.inorgchem.5b00578.
(44) Schlachter, A.; Tanner, K.; Harvey, P. D. Copper Halide-Chalcogenoether and -Chalcogenone Networks: Chain and Cluster Motifs, Polymer Dimensionality and Photophysical Properties. *Coordination Chemistry Reviews* **2021**, *448*, 214176. https://doi.org/10.1016/j.ccr.2021.214176.
(45) Keller, S.; Prescimone, A.; Bolink, H.; Sessolo, M.; Longo, G.; Martínez-Sarti, L.; Junquera-Hernández, J. M.; Constable, E. C.; Ortí, E.; Housecroft, C. E. Luminescent Copper(I) Complexes with Bisphosphane and Halogen-Substituted 2,2′-Bipyridine Ligands. *Dalton Trans.* **2018**, *47* (40), 14263–14276. https://doi.org/10.1039/C8DT01338A.
(46) Keller, S.; Bantle, M.; Prescimone, A.; Constable, E. C.; Housecroft, C. E. Hinged and Wide: A New P^P Ligand for Emissive [Cu(P^P)(N^N)][PF6] Complexes. *Molecules* **2019**, *24* (21), 3934. https://doi.org/10.3390/molecules24213934.
(47) Xu, K.; Chen, B.-L.; Yang, F.; Liu, L.; Zhong, X.-X.; Wang, L.; Zhu, X.-J.; Li, F.-B.; Wong, W.-Y.; Qin, H.-M. Largely Color-Tuning Prompt and Delayed Fluorescence: Dinuclear Cu(I) Halide Complexes with *Tert* -Amines and Phosphines. *Inorg. Chem.* **2021**, *60* (7), 4841–4851. https://doi.org/10.1021/acs.inorgchem.0c03755.

(48) Kobayashi, A.; Arata, R.; Ogawa, T.; Yoshida, M.; Kato, M. Effect of Water Coordination on Luminescent Properties of Pyrazine-Bridged Dinuclear Cu(I) Complexes. *Inorg. Chem.* **2017**, *56* (8), 4280–4288. https://doi.org/10.1021/acs.inorgchem.6b02578.
(49) Bassoli, S.; Ardizzoia, G. A.; Therrien, B.; Brenna, S. Phosphorescence Enhancement by Close Metal–Metal Interaction in T 1 Excited State in a Dinuclear Copper (i) Complex. *Dalton Transactions* **2019**, *48* (25), 9276–9283.
(50) Sun, C.; Llanos, L.; Arce, P.; Oliver, A.; Wannemacher, R.; Cabanillas-Gonzalez, J.; Lemus, L.; Aravena, D. Nuclearity Control for Efficient Thermally Activated Delayed Fluorescence in a Cu ^{I} Complex and Its Halogen-Bridged Dimer. *Chem. Mater.* **2021**, *33* (16), 6383–6393. https://doi.org/10.1021/acs.chemmater.1c01531.
(51) Artem'ev, A. V.; Demyanov, Y. V.; Rakhmanova, M. I.; Bagryanskaya, I. Y. Pyridylarsine-Based Cu (I) Complexes Showing TADF Mixed with Fast Phosphorescence: A Speeding-up Emission Rate Using Arsine Ligands. *Dalton Transactions* **2022**, *51* (3), 1048–1055
.

Graphical abstract:

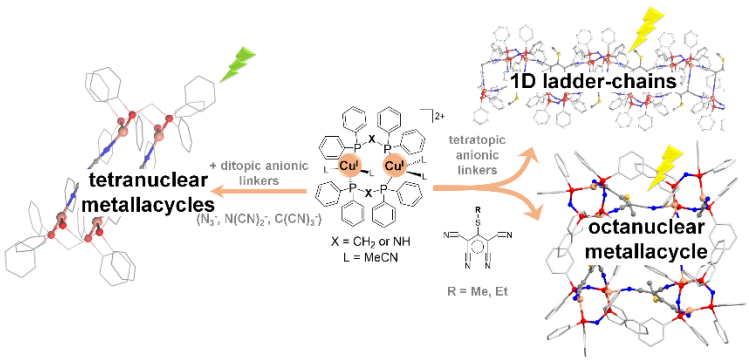

Bimetallic Cu(I) building blocks react with pseudohalide ligands to form luminescent polymetallic assemblies whose various architectures can be rationalized considering intra- and inter- molecular interactions.